Determining rock crack stress thresholds using ultrasonic through-transmission measurements

Jiangwan He[1] · Mehdi Serati[1] · Martin Veidt[2] · Arthur De Alwis[1]

Abstract

The crack initiation stress threshold is widely used in excavation industries as rock spalling strength when designing deep underground structures to avoid unwanted brittle failures. While various strain-based methods have been developed for the estimation of this critical design parameter, such methods are destructive and often requires subjective interpretations of the stress–strain curves, particularly in rocks with pre-existing microcracks or high porosity. This study explore the applicability of non-destructive ultrasonic through-transmission methods for determining rock damage levels by assessing the changes in transmitted signal characteristics during loading. The change in velocity, amplitude, dominant frequency, and root-mean-square voltage are investigated with four different rock types including marble, sandstone, granite, and basalt under various stress levels. Results suggest the rate of signal variations can be reliably used to estimate crack closure and crack initiation stress levels across the tested rocks before failure. Comparison of the results between the conventional techniques and the new proposed methods based on ultrasonic monitoring are further discussed.

1 Introduction

With the development of advanced excavation techniques and state-of-the-art equipment, underground structures and mining facilities are being constructed at increased depths. The depth of Shakhterskaya coal mine in Europe, for instance, is nearly 1500 m while the Mponeng gold mine in South Africa is reaching beyond 4000 m (Ranjith et al. 2017). At depth, the induced stress field around excavations increases due to gravitational loads leading to more unwanted brittle rock failures like spalling, slabbing, and rockburst (Nicksiar and Martin 2012; Masoumi et al. 2017). Such rock failures (mainly observed in low porosity and highly crystalline formations) are formed through the generation of new and/or extension of pre-existing microcracks in directions parallel to the maximum induced hoop stress. Thin slabs and large flakes or sometimes V-shaped notches

could also be formed where coupled tensile and shear zones are created. Spallinge-like explosive failures exhibit a highly energetic nature and are typically characterised by minimal or negligible plastic deformation prior to rock disintegration. The ejection speed of fragments during rock spalling can easily reach velocities of up to 10 m/s, making it a very powerful rupture. Laboratory and field assessments of damage evolution in brittle rocks are therefore a necessity for the design and safe operation of civil and mining infrastructures in deep environments (Fairhurst and Cook 1966; Ortlepp and Stacey 1994; Serati et al. 2015; Keneti and Sainsbury 2018; Serati et al. 2022a, b).

As supported by various references (Bieniawski 1967; Brace et al. 1966; Diederichs 2007; Lajtai 1974; Martin and Chandler 1994; Nicksiar and Martin 2012; Stacey 1981), the fracture processes observed in low-porosity rocks under the Unconfined Compressive Strength (UCS) test condition involve several distinct stages, including: (i) The crack closure (CC) stage, characterised by an initial non-linear region where the axial stiffness also increases due to the closure of pre-existing microcracks in the rock matrix, (ii) the elastic stage during which deformation is directly proportional to the applied stress, (iii) the crack initiation (CI) zone where new microcracks are generated under stable crack growth

✉ Mehdi Serati
 mehdi.serati@uq.edu.au

1 School of Civil Engineering, The University of Queensland, Brisbane, QLD 4072, Australia

2 School of Mechanical and Mining Engineering, The University of Queensland, Brisbane, QLD 4072, Australia

conditions resulting in irreversible damage to the rock, i.e. additional load is required to extend the crack length, (iv) the crack damage (CD) stress level where rock experiences unstable crack growth. At this stage, the extension of microcracks becomes unpredictable and independent of the applied load, and (v) final rock failure. Among these stress thresholds, it is widely acknowledged and supported by numerous case histories that CI stress can serve as an indicator of the in-situ spalling strength of rock. Typically, this threshold is recognised to be approximately 30% to 60% of UCS. It is also suggested that both CI and CD are inherent material parameters, remaining largely unaffected by factors such as loading rate, sample size, or other test-dependent variables (Cai and Kaiser 2014; Martin and Christiansson 2009; Martin et al. 1999). Several strain-based methods have, therefore, been proposed to determine these critical crack stress levels. This includes the Volumetric Strain (VS) method, introduced by Brace et al. (1966), the Lateral Strain (LS) method, proposed by Lajtai (1974), the Extensional Strain (ES) method, put forth by Stacey (1981), the Crack Volumetric Strain (CVS) method, developed by Martin and Chandler (1994), the Poisson's Ratio (PR) method, proposed by Diederichs (2007) and the Lateral Strain Response (LSR) Method introduced by Nicksiar and Martin (2012).

However, despite being widely used, the above stress–strain techniques rely on the quality of strain gauge installation and necessitate visual interpretation of plot data, which can introduce significant errors and high-level of human subjectivity (Zhao et al. 2015). For instance, Martin and Chandler (1994) noticed difficulties in employing Volumetric Strain Methods when specimens contain a high density of pre-existing microcracks. Eberhardt et al. (1998) highlighted that assuming a single value for the elastic constant in the Crack Volumetric Strain Method can lead to substantial variation and uncertainty. Additionally, Andersson et al. (2009) noted that the Extensional Strain Method often fails to produce a true linear region, particularly with modern data acquisition techniques that offer higher resolution. In addition, these methods require laboratory testing using destructively sampled rock which imposes further limitations on sample size and testing conditions due to equipment availability. Non-Destructive Testing (NDT) methods are becoming more preferred in recent years to evaluate the extent of rock damage and monitor fracture behaviour without compromising functionality or causing additional harm to rock samples.

Amongst various NDT techniques employed for rock damage characterisation, acoustic emissions (AE) (Chang and Lee 2004; Kim et al. 2015; Li and Einstein 2017; Li et al. 2019; Wu et al. 2021), ultrasonic testing (Modiriasari et al. 2017; Shirole et al. 2020a; Wu et al. 2023), electrical impedance spectroscopy (EIS) (Saltas et al. 2014; Yin and Xu 1997), digital image correlation (DIC) (Shirole et al.

2020b), high-speed photography (Serati et al. 2012, 2014), and computed tomography (CT) scanning (Shuai et al. 1997) are widely adopted. Ultrasonic testing is a dynamic NDT method that utilises various transducer and receiver configurations to propagate ultrasonic stress waves into the material under examination. This technique involves analysing the elastic wave characteristics and signal behaviours resulting from wave reflection, deflection, diffraction, scattering, cross modulations of excitations, and generation of higher harmonics. While commonly applied to metals or concrete, ultrasonic methods have also been adapted for damage characterisation and defect detection purposes in rock engineering. Ultrasonic testing mainly focuses on identifying the position, orientation, and size of defects in a static state. This involves employing amplitude techniques that correlate flaw size and location with signal amplitude, temporal techniques that analyse arrival times, and imaging techniques that scan the material along different directions using a single probe or phased array probes (Felice and Fan 2018). In essence, ultrasonic testing serves as an active NDT method that enables the comprehensive evaluation of materials by leveraging the behaviour of ultrasonic stress waves. If higher-order harmonics and nonlinear interactions between ultrasonic waves within the material are of interest, non-linear ultrasonic techniques should be used. For simpler problems, however, linear ultrasonic methods through transmission pulses of compressional (P-wave) and/or shear (S-wave) waves are alternatively employed to evaluate the damage state of materials.

Mainly using linear ultrasonic techniques, correlations between ultrasonic parameters and various rock properties such as UCS, porosity, density, static modulus, and dynamic modulus are available (Chawre 2018; Entwisle et al. 2005). For instance, rock samples with higher porosity, lower density, and a greater density of microcracks exhibit a reduction in velocity accompanied by a decrease in the amplitude of the transmitted wave. Or, several studies have indicated that the P-wave velocity measured perpendicular to the orientation of cracking shows higher sensitivity to crack initiation and accumulation compared to the P-wave velocity measured along the direction of the major principal stress (Eberhardt et al. 1998; Ghazvinian 2015). These findings highlight the potential of ultrasonic techniques to provide valuable insights into the progression of damage in rocks, particularly by utilising measurements perpendicular to the cracking orientation. Wulff et al. (1999) and Yang et al. (2018) found that the P-wave velocity and attenuation exhibit higher sensitivity than the S-wave, showing an earlier response to the crack initiation and more variations during the damage process. Nur and Simmons (1969) noted that moisture and confinement have a more significant impact on P-wave velocity compared to S-wave velocity. Yin and Xu (2020)

suggested both ultrasonic velocity and amplitude attenuation can be used to indicate the degree of damage with amplitude attenuation being more sensitive to the damage, indicated by a significant drop close to CD stress threshold and a larger overall drop compared to the velocity indicator. Garg et al. (2019) and Modiriasari et al. (2017) also found that the ultrasonic amplitude can detect crack initiation and growth in pre-cracked samples earlier than DIC methods. More recent studies investigated the feasibility of using ultrasonic methods to characterise the crack damage stress thresholds. Ghazvinian (2015) tested marble and granite under uniaxial and triaxial condition and found that the stress at which maximum lateral P-wave velocity occurs close to the CI stress threshold determined using the stress–strain method and AE methods. Further investigations by Shirole et al. (2020a) suggested both amplitude and dominant frequency analysis of the response signal could be used to characterise the CI and CD stress threshold, while an excitation frequency of 5 MHz or higher is preferred for sandstone samples to ensure adequate sensitivity. In addition, wavelet packet decomposition and intrinsic attenuation analysis of the ultrasonic signal also show potential in characterising the crack damage stress thresholds for rock (Dai et al. 2023).

However, the majority of linear ultrasonic testing techniques employed for characterising rock damage primarily rely on velocity and amplitude as indicators, while the exploration of the frequency spectrum and total energy of the ultrasonic signal during rock fracture propagation remains inconclusive. This study aims to delve deeper into the feasibility and accuracy of utilising ultrasonic through-transmission methods for determining the stress thresholds associated with crack damage in four different rock types. The investigation focuses on analysing the ultrasonic signal characteristics and behaviours under uniaxial compressive loading, with specific emphasis on wave velocity, wave amplitude, dominant frequency, and root-mean-square voltage (VRMS).

2 Experiment design

Ultrasonic signal behaviour and strain response during uniaxial compression tests with four different rock types (basalt, granite, marble, and sandstone) are investigated in the present work (see Fig. 2). The selection of these rock types was made to include a wide range of porosity and strength values, ensuring a comprehensive analysis. Cylindrical samples were prepared in accordance with the suggested methods by the International Society for Rock Mechanics (ISRM) (Bieniawski and Bernede 1979). To minimise unwanted moisture effects on the measurements, samples were first oven-dried for 48 h at 105 ° C and then stored in sealed bags prior to conducting ultrasonic and strain measurements. Key properties of tested rocks, including diameter, length, density, porosity, grain size, UCS, and ultimate tensile strength (UTS) are summarised in Table 1. Additionally, microscopic images for each rock type are shown in Fig. 1.

To investigate the influence of the ultrasonic transducer's central frequency on the results, a series of preliminary ultrasonic tests were initially conducted on each rock sample without applying external loading. Olympus Centrascan transducers with different central frequencies of 1 MHz, 2.25 MHz, 5 MHz, and 10 MHz were selected for this purpose. The selection of Centrascan transducers was based on several specific advantages including their high sensitivity (which allows for accurate detection of even small signals), their ability to minimise interference from background reflections, their wider frequency bandwidth (enabling them to capture a broader range of signals) as well as their higher signal-to-noise ratio, ensuring the quality and reliability of the acquired data (Olympus 2019). A coupling medium of "molasses" honey was preferred for its high viscosity and stickiness to ensure a stable and robust connection between the transducer and the rock interface and to minimise the potential for slip and detachment during the experiment. The high acoustic impedance of honey also helps in testing rocks with
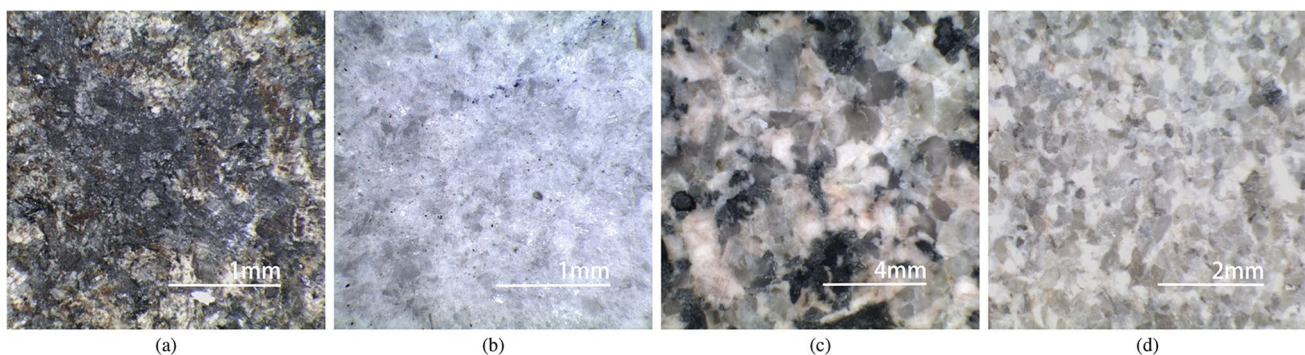

Fig. 1 Microscopic images for **a** Basalt, **b** Marble, **c** Granite, and **d** Sandstone
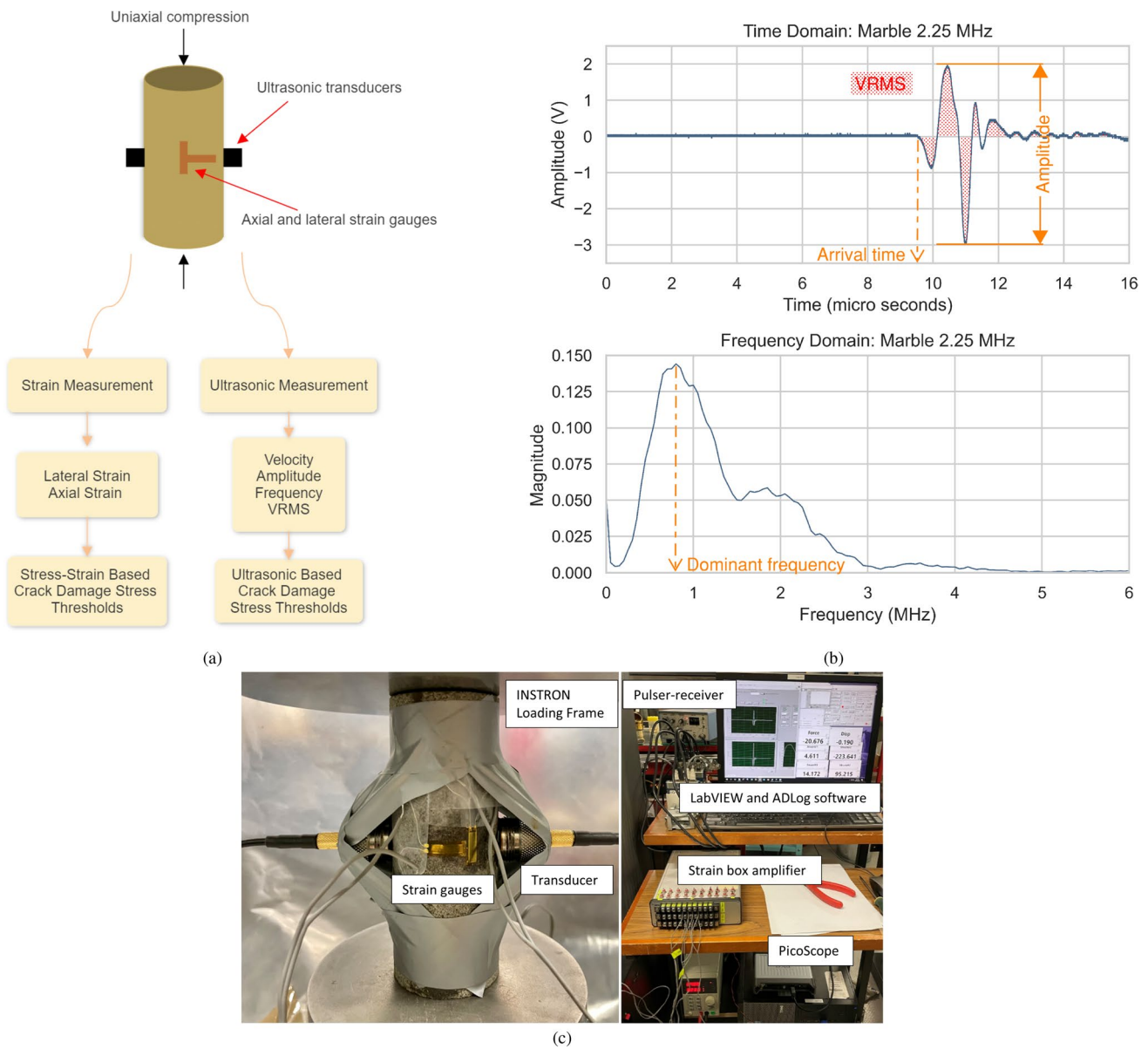
(a)

(b)

(c)

Fig. 2 **a** Schematic representation of the testing procedure, **b** Ultrasonic signal in both time and frequency domains with arrival time, amplitude, dominant frequency, and VRMS definitions marked on the graph, and **c** Experimental setup for ultrasonic monitoring during UCS tests

Table 1 Specifications of tested rock samples

Rock type	Diameter (mm)	Length (mm)	Density (kg/m^3)	Porosity (%)	Grain size (μm)	UCS (MPa)	UTS (MPa)
Basalt	39.40	104.50	2577 ± 13	7.15 ± 0.16	53 ± 19	144.4 ± 1.7	8.5 ± 2.1
Granite	39.60	98.00	2621 ± 6	0.57 ± 0.02	684 ± 362	194.2 ± 0.7	9.5 ± 0.9
Marble	39.50	104.80	2696 ± 4	0.17 ± 0.05	57 ± 21	99.3 ± 5.7	7.3 ± 1.0
Sandstone	55.20	141.70	2181 ± 2	16.27 ± 0.15	203 ± 97	45.8 ± 0.6	3.3 ± 0.6

rough surfaces and high attenuation to mitigate impedance mismatch. The testing setup involved an Olympus Model 5077PR Pulser-Receiver to generate square wave excitation, with the pulse width adjusted for each transducer central frequency (see Fig. 2c). To mitigate the interference caused by the near field and trigger pulse, a through transmission test configuration was implemented with all transducers.

From the time-amplitude graphs and measurements of the arrival time summarised in Table 2 and Fig. 3, it is evident that the first wave arrives faster as the frequency increases from 1 to 5 MHz across all tested rock types. When the transducer frequency is raised to 10 MHz, the wave velocity experiences further acceleration, specifically in basalt, granite, and marble. This trend of increasing velocity with higher transducer frequency has also been previously reported in the literature (Cadoret et al. 1995; Shirole et al. 2020a). However, unlike granite and basalt, sandstone and marble also exhibit the generation of higher harmonics at multiples of the dominant frequency when subjected to testing with 1 MHz and 2.25 MHz transducers. Across all tested rock types, the dominant frequency of the transmitted wave falls within the range of 0.4–1.8 MHz. It can be seen that the relationship between the dominant frequency and the transducer central frequency is not linear, which also aligns with previous findings (Shirole et al. 2020a; Pyrak-Nolte et al. 1990). In all cases, a significant reduction of the dominant frequency is pronounced after transmission which indicates a strong low-pass effect, meaning a small portion of higher frequencies can only be transmitted through the microstructure without significant attenuation. Marble with the lowest porosity, highest density, and relatively smooth and homogeneous microstructure produces the highest dominant frequency regardless of the transducer frequency used. Sandstone with the lowest density and highest porosity produces the lowest dominant frequency. For granite with large grain size and nonhomogeneous, non-uniform appearance, the dominant frequency is governed by its microstructure and is independent of the transducer at high frequency ranges. Such frequency dependency of wave attenuation and time delay across a discontinuity has also been reported by Pyrak-Nolte et al. (1990) and Shirole et al. (2020b). Higher transducer frequency with smaller wavelength is more sensitive to the size and distribution of voids, cracks and other small-scale heterogeneities in rock. The smaller wavelength has a better detectability for small defects, while higher frequency signal experiences more energy dispersion, resulting in more significant attenuation and changes in wave velocity. Therefore, higher frequencies are typically preferred for monitoring microscopic changes in rock. These observations strongly emphasise the importance of selecting an appropriate transducer with adequate bandwidth and a high signal-to-noise ratio for crack monitoring in rock formations. Such considerations ensure a careful balance between accuracy and sensitivity, ultimately enabling optimal performance within the desired frequency range. It was also observed that the size of the transducer element has a minimum effect on the arrival time, but a larger gain is often needed for smaller element size due to reduced total energy resulted from smaller transmission area. In addition, the velocity and dominant frequency for each specimen within a rock type exhibited high consistency, with less than 5% Coefficient of Variation (CoV) for the velocity and less than 14% CoV for the dominant frequency. Therefore, it is safe to assume each specimen has a similar ultrasonic characteristic and can be used to generalise the ultrasonic behaviour for a specific rock type.

A pair of 2.25 MHz (Olympus C540-SM P-wave) transducers were finally selected in this study based on the above preliminary results. Transducers were coupled at mid-height of the specimen using insulation tape. The ultrasonic wave was transmitted in the lateral direction across the diameter of the sample, while the vertical axis was connected to the loading platens acting as the major principal axis. The same
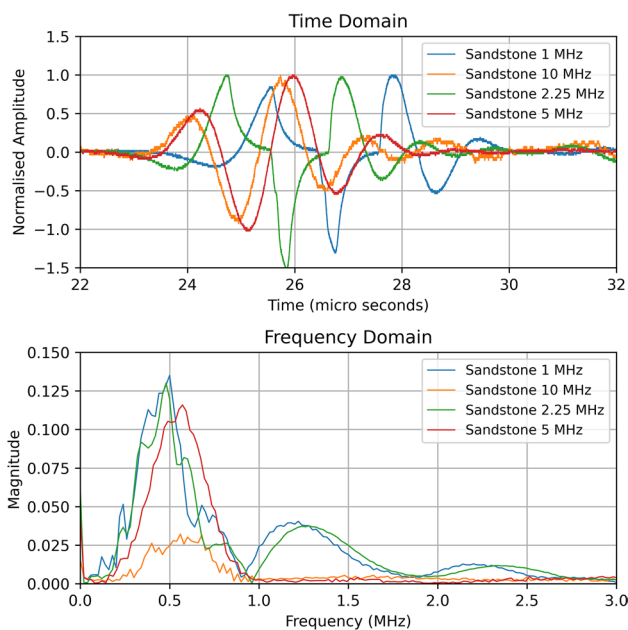

Fig. 3 Comparison of the transmitted signal for different transducer frequencies

Table 2 First wave arrival time for different transducer central frequencies	Frequency (MHz)	P-wave velocity (m/s)				Dominant frequency (MHz)			
		Basalt	Granite	Marble	Sandstone	Basalt	Granite	Marble	Sandstone
	1	4,604	4,975	3,919	2,338	0.85	0.65	0.9	0.50
	2.25	4,842	5,335	4,122	2,411	0.75	0.6	0.8	0.48
	5	4,967	5,530	4,194	2,443	0.8	0.55	1.6	0.57
	10	4,968	5,565	4,195	2,408	0.9	0.8	1.8	0.56

"molasses" honey was used as the coupling medium and the excitation voltage of the Pulser-Receiver was set to 400 V. A pulse repetition frequency (PRF) of 200 Hz was utilised to guarantee that each pulse reaches the receiver before sending the next pulse. Ultrasonic signals were collected continuously at 0.5 Hz using LabVIEW based automated measurement interface and PicoScope 5000 series USB oscilloscope. The sampling rate of the PicoScope was set to 125 MHz to ensure adequate resolution while filter out the noise by averaging 8 samples. The arrival time of the transmitted signal was defined as the point when the wave amplitude first deviated from zero, rather than the time of peak amplitude, to eliminate the influence of changing periods at different stress levels. The frequency spectrum and dominant frequency of the initial transmitted signal were then determined using the fast Fourier transform (FFT) performed in the vicinity of the first transmitted signal.

As illustrated in Fig. 2, both strain and active ultrasonic measurements were carried out in-sync with the uniaxial compressive loading for each rock sample. An Instron-5985 250 kN loading frame was used under load-controlled condition at 200 N/s. Four strain gauges (BA 120-10AA /120 Ohm) were attached at mid-height of the sample, with two of them oriented laterally and two of them oriented vertically, to obtain both axial and horizontal normal strain. The voltage output signal from the amplifier was read by NI 9215 Analogue module connected to a laptop with ADlog software for data logging. Sample frequency for ADlog was selected to be 10 Hz, with force, displacement, and four strain measurements from the Instron loading frame and strain gauge amplifier recorded. The change in P-wave velocity, wave amplitude, dominant frequency, and root-mean-square voltage (VRMS) during the loading process was then analysed in Python, and is discussed in the next Section. In addition, UCS, Young's modulus, Poisson's ratio, and crack damage stress thresholds were determined for each sample using the six previously explained stress–strain methods in Sect. 1.

3 Results and discussion

Tables 3 and 4, and Fig. 4 provide a summary of the obtained measurements using the stress–strain methods detailed in the previous section. It is clear that the Volumetric Strain method (VS) generally yields lower values for both CC and CI compared to the other methods. For marble, granite, and sandstone, the graphs obtained from the Lateral Strain Method and Extensional Strain Method often exhibit a significant nonlinear nature (Andersson et al. 2009), making it challenging to identify precise values for CC and CI. The LSR Method, although it tends to provide higher CI values, exhibits a smaller CoV and involves less subjectivity, hence

is considered to be the most consistent and the least subjective technique (Nicksiar and Martin 2012; Zhang et al. 2021; Zhao et al. 2013; Koosmen et al. 2023).

At the next step, recorded ultrasonic signals were analysed in terms of their travel time and amplitude using signal processing tools in Python. Through careful analysis of the collected signals, it was evident that the change in wave velocity at different stages of uniaxial loading follows a similar trend across all specimens of the same rock type. This has also be reported elsewhere (Shirole et al. 2020a; Modiriasari et al. 2017; Wulff et al. 1999; Stanchits et al. 2006; Garg et al. 2019; Pellet and Fabre 2007; Ghazvinian 2015). However, when comparing different rock types, notable variations in their wave velocity behaviours become apparent, exemplified by the distinct trends illustrated by the green lines in Fig. 5. For instance, the wave velocity remains initially unchanged for basalt specimens, then starts to decrease at an accelerating rate. This trend suggests vertically oriented pre-existing microcracks in basalt, leading to lateral dilation and expansion under axial loading, bypassing the crack closure stage (Ji et al. 2018). The inherent properties of basalt, characterised by a low Young's modulus and high Poisson's ratio, further contribute to continuous lateral expansion, causing a reduction in velocity. In contrast, marble specimens demonstrate a continuous increase in velocity until reaching approximately 75% UCS. This distinct behaviour is attributed to marble having the lowest porosity, highest density, and a smaller grain size compared to other rock types, resulting in a compacted medium with minimal pre-existing microcracks. The generation of small-sized microcracks during loading is challenging to detect with lower-frequency transducers. Furthermore, the highest Young's modulus and lowest Poisson's ratio indicate minimal lateral dilation. Consequently, the reduction in velocity due to microcracking and lateral dilation is insignificant and challenging to detect, compared to the significant increase in velocity caused by the compression of grains and pores. On the other hand, granite, and sandstone display a rising trend in ultrasonic velocity until around 36%–56% UCS before rapidly declining. This initial increase is indicative of the closure of pre-existing microcracks under axial compression. However, further compression leads to the generation of new microcracks at grain boundaries, resulting in a subsequent reduction in velocity. Sandstone, having the highest porosity and lowest density, initially exhibits enhanced crack closure effects due to greater susceptibility to compressive forces. However, its subsequent behaviour involves significant lateral dilation supported by the largest Poisson's ratio, contributing to a more pronounced decrease in ultrasonic velocity compared to other rock types.

The variation of wave velocity among different rock types does not demonstrate a consistent trend. However, a general trend becomes apparent when analysing the derivatives
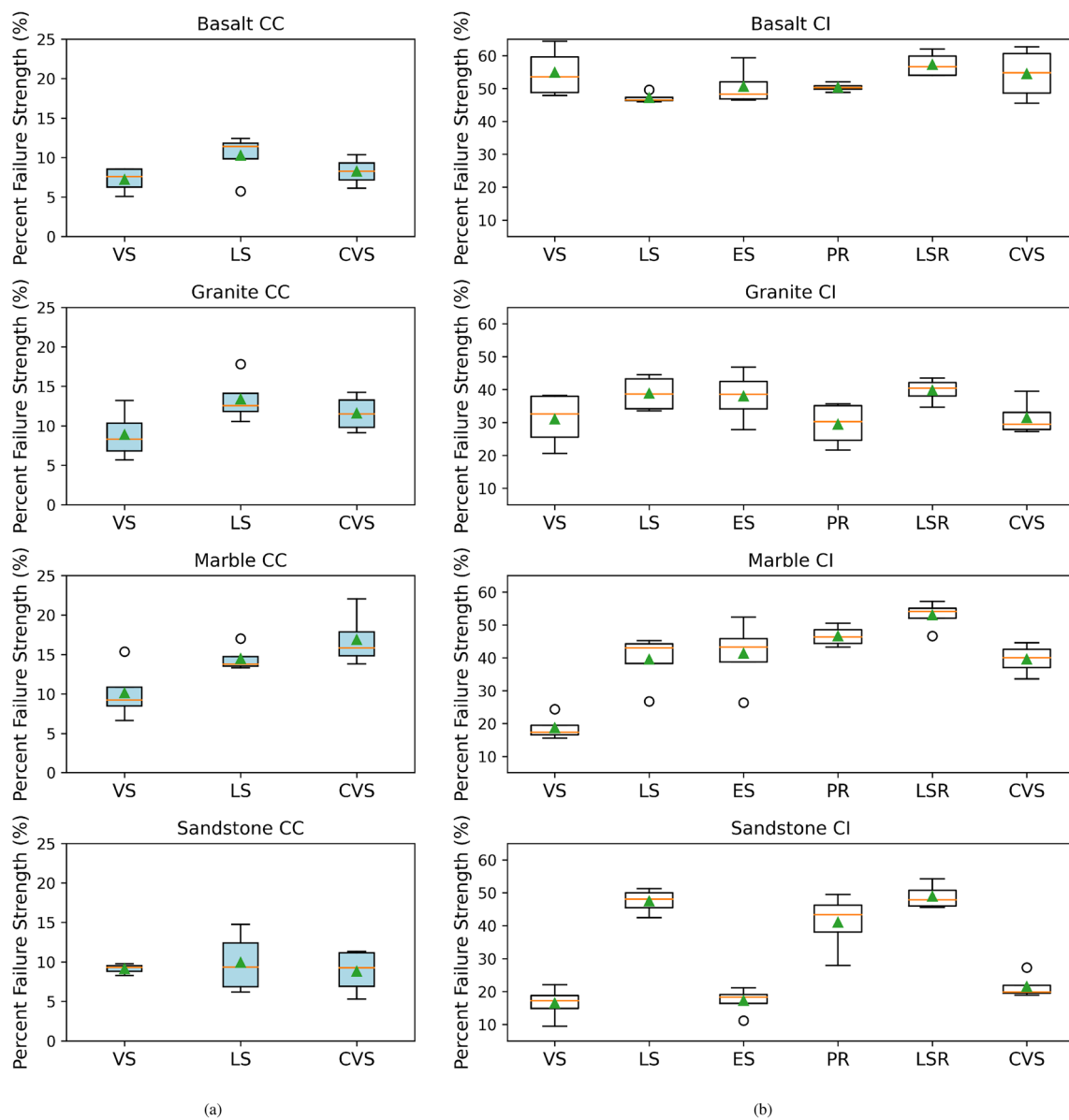
Fig. 4 Box plot comparison of the **a** Crack closure (CC) and **b** Crack initiation (CI) stress thresholds determined using conventional stress–strain techniques, including Volumetric Strain (VS), Lateral Strain (LS), Extensional Strain (ES), Poisson's Ratio (PR), Lateral Strain Response (LSR), and Crack Volumetric Strain (CVS) methods. Median and mean values are indicated by a horizontal orange line and a green triangle, respectively

Table 3 Average and SD of the CC and CI stress thresholds determined using conventional stress–strain methods

Rock type	CC (% UCS)			CI (% UCS)					
	VS	LS	CVS	VS	LS	ES	PR	LSR	CVS
Basalt	7.2 ± 1.4	10.3 ± 2.6	8.3 ± 2.1	54.8 ± 6.7	47.2 ± 1.4	50.6 ± 5.2	50.3 ± 1.1	57.3 ± 3.4	54.4 ± 7.1
Granite	8.9 ± 2.8	13.4 ± 2.7	11.6 ± 2.1	31.0 ± 7.4	38.8 ± 4.9	38.0 ± 6.9	29.4 ± 6.0	39.7 ± 3.3	31.4 ± 4.8
Marble	10.1 ± 3.2	14.5 ± 1.5	16.9 ± 3.1	18.7 ± 3.4	39.5 ± 7.5	41.3 ± 9.4	46.6 ± 2.8	53.0 ± 3.9	39.6 ± 4.1
Sandstone	9.1 ± 0.6	9.9 ± 3.5	8.8 ± 2.5	16.5 ± 4.5	47.5 ± 3.4	17.2 ± 3.7	41.0 ± 8.1	48.9 ± 3.5	21.5 ± 3.4

Table 4 Summary of UCS test results and crack damage stress thresholds using stress–strain based techniques

Rock type	v	E_{av} (GPa)	CC (%)	CI (%)	CD (%)
Basalt	0.23 ± 0.01	49.4 ± 0.8	9 ± 1	52 ± 3	88 ± 2
Granite	0.20 ± 0.05	55.4 ± 2.0	11 ± 2	35 ± 5	85 ± 8
Marble	0.19 ± 0.01	63.6 ± 1.6	14 ± 1	40 ± 2	85 ± 4
Sandstone	0.40 ± 0.11	38.9 ± 2.7	9 ± 1	34 ± 3	86 ± 5

(rate of change) of the velocity. As depicted by the red lines in Fig. 5, regardless of the rock type, the derivative graph displays an increasing trend after the commencement of the loading, reaching its peak in proximity to the CC stress threshold. The observed peak in the derivative graph suggests fastest increase in velocity, attributed to the closure of pre-existing microcracks under uniaxial compression, resulting in a compacted medium for the ultrasonic wave to travel through. Subsequently, after reaching the maximum

derivative, the rate of velocity increase diminishes linearly, signifying the termination of crack closure. Instead, factors causing velocity decrease, such as lateral dilation, become more pronounced. Similarly, the transition from the first linear region to the second linear region indicates a shift to a slower rate of velocity increase, caused by the onset of stable crack growth and more pronounced lateral expansion. Therefore, the intersection of the two linear regions can be used to characterise the CI stress threshold.

While wave velocity and wave amplitude are separate properties of an ultrasonic wave, it is often noted that the change in amplitude often follows a similar trend to the change in velocity for each rock type. To verify this, the amplitude of ultrasonic signals was calculated by finding the difference between the maximum and minimum values in the signal, then normalised based on the initial amplitude before loading. As illustrated by the green lines in Fig. 6, the wave amplitude is increasing at the beginning of the loading process, attributed to the closure of pre-existing microcracks,
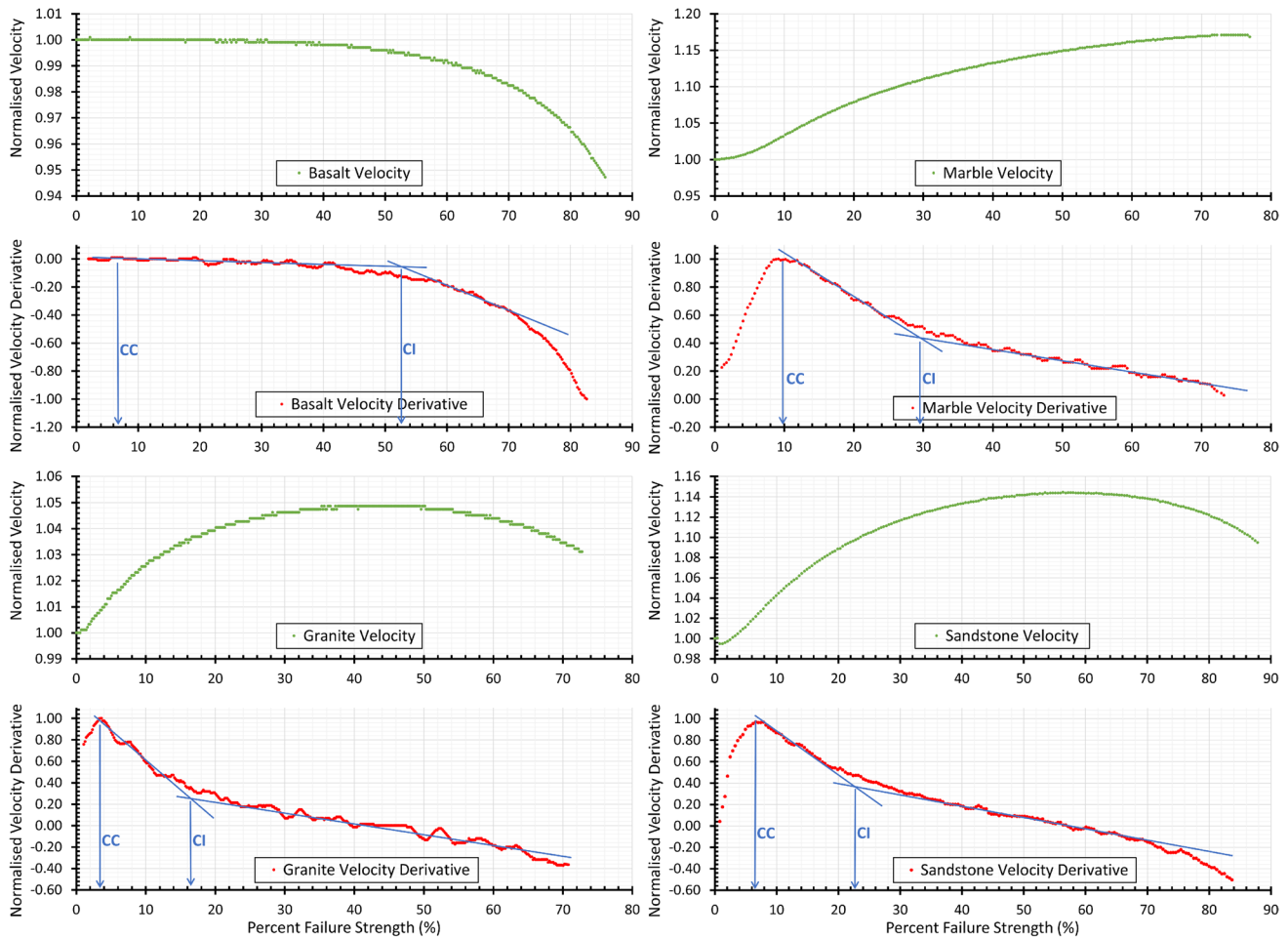

Fig. 5 Change in ultrasonic velocity (green lines) and velocity derivatives (red lines) during uniaxial loading for basalt (top left), marble (top right), granite (bottom left), and sandstone (bottom right) sam-

ples. The CC and CI stress thresholds are determined using blue reference lines on the derivative graphs
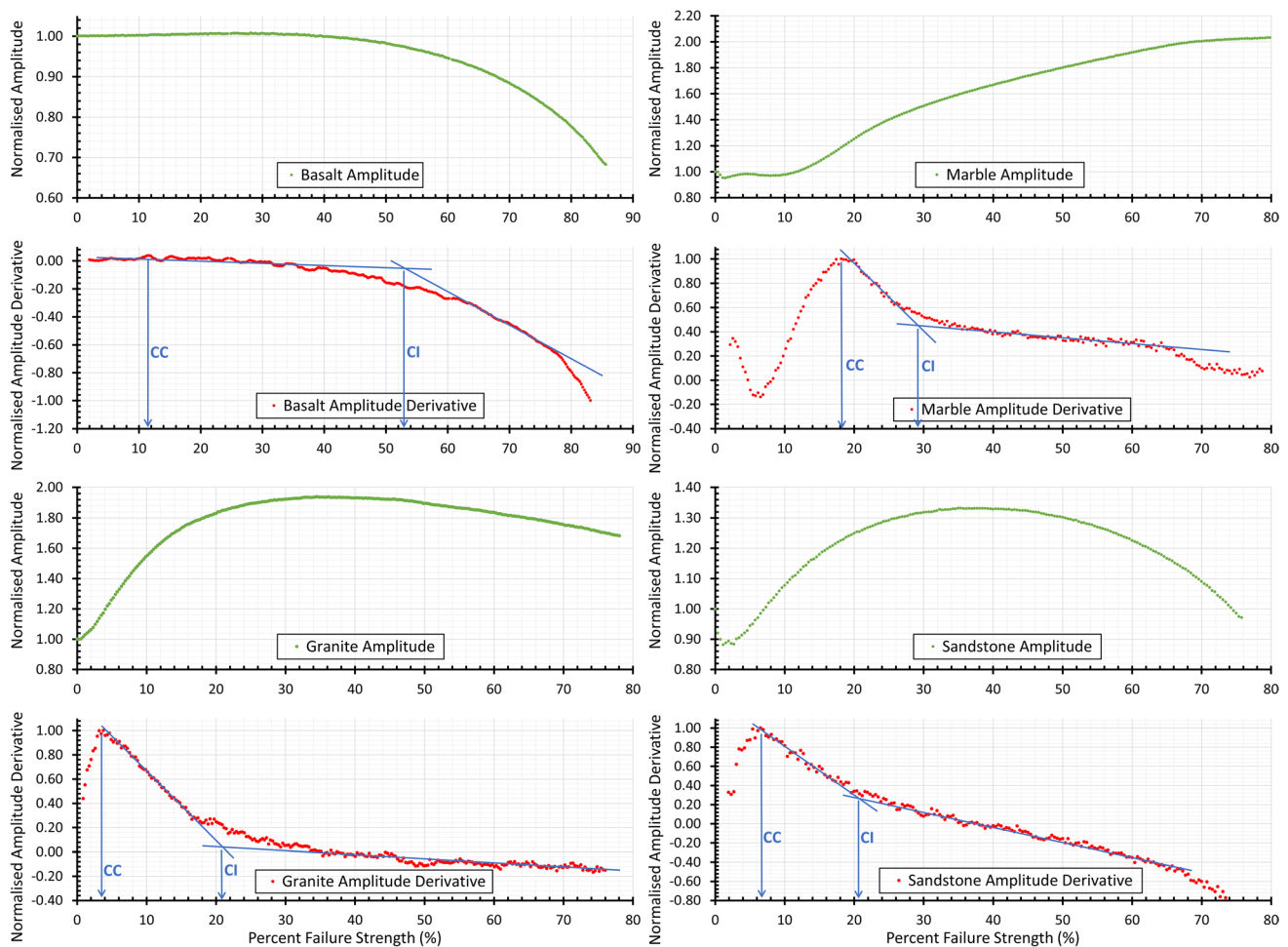
Fig. 6 Change in wave amplitude (green lines) and amplitude derivatives (red lines) during uniaxial loading for basalt (top left), marble (top right), granite (bottom left), and sandstone (bottom right) samples. The CC and CI stress thresholds are determined using blue reference lines on the derivative graphs

voids, and air gaps within the rock. This closure can lead to increased contact between adjacent grains, reducing the scattering and energy dissipation of the ultrasonic wave. Consequently, a more compact medium is created, facilitating the transmission of the ultrasonic wave with higher amplitude. Similar to the velocity derivative graph, it was observed that the point at which the maximum amplitude derivative occurs can be used to characterise the CC stress threshold. Following crack closure, as the rock enters the linear elastic region, the wave amplitude continues to increase but at a diminishing rate, as indicated by the first linear region in the derivative graph after the CC. Beyond the CI stress threshold, the amplitude either increases more slowly or decreases more rapidly due to the accumulated attenuation resulting from the generation of new microcracks. Consequently, the intersection of the first and second linear regions in the derivative graph can be used to characterise the CI stress threshold. The similarity between the amplitude derivative and velocity derivative further reinforces the validity of using derivatives

to characterise the damage process. Additionally, the wave amplitude experiences a maximum change of 120% during the loading process, whereas the ultrasonic velocity only exhibits a maximum change of 20%. This indicates that the amplitude is more sensitive to microscopic changes in the rock compared to the ultrasonic velocity.

The next step involved performing frequency analysis of the received signal using Fast Fourier Transformation (FFT) in Python. By identifying the frequency with the highest spectral amplitude, the dominant frequency was determined. Throughout the uniaxial loading process, continuous monitoring of the change in dominant frequency was carried out. However, unlike the velocity and amplitude charts, the change in the dominant frequency doesn't show a distinct trend, as depicted in Fig. 7. This observation aligns with the findings reported by Dai et al. (2023) that the lack of a clear trend in the dominant frequency change may be attributed to the Nyquist frequency limit imposed by the experimental setup. The results of spectral analysis may therefore vary
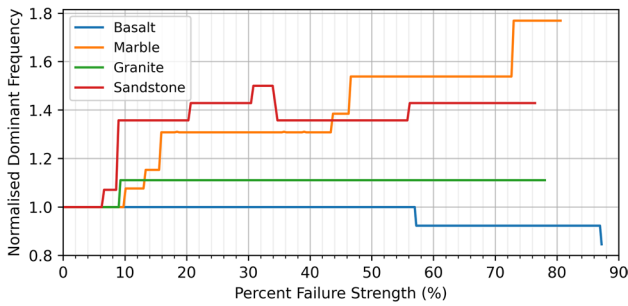
Fig. 7 Variation in the dominant frequency at different stages of uniaxial loading for all tested rock types

even for the same rock types depending on the sampling frequency, number of samples, and transducer frequencies used; hence cannot be considered as a general recipe to identify crack damage evolution in rock.

Finally, the root-mean-square voltage (VRMS)—defined as the square root of the average value of the instantaneous voltage according to Eq. (1)—was measured. The VRMS gives the equivalent voltage for complex waveform by considering the amplitude of the first received wave at all time steps, hence accounts for the effect from both the changing amplitude and the changing frequency. The change in VRMS as shown in Fig. 8 exhibits a similar trend to the change in amplitude and velocity for each rock type.

$$V_{\rm rms} = \sqrt{\frac{1}{T} \int_0^T V(t)^2 \mathrm{d}t} \tag{1}$$

Figure 9, along with Table 5, provides a comprehensive statistical comparison between the CC and CI stress thresholds determined using conventional stress–strain
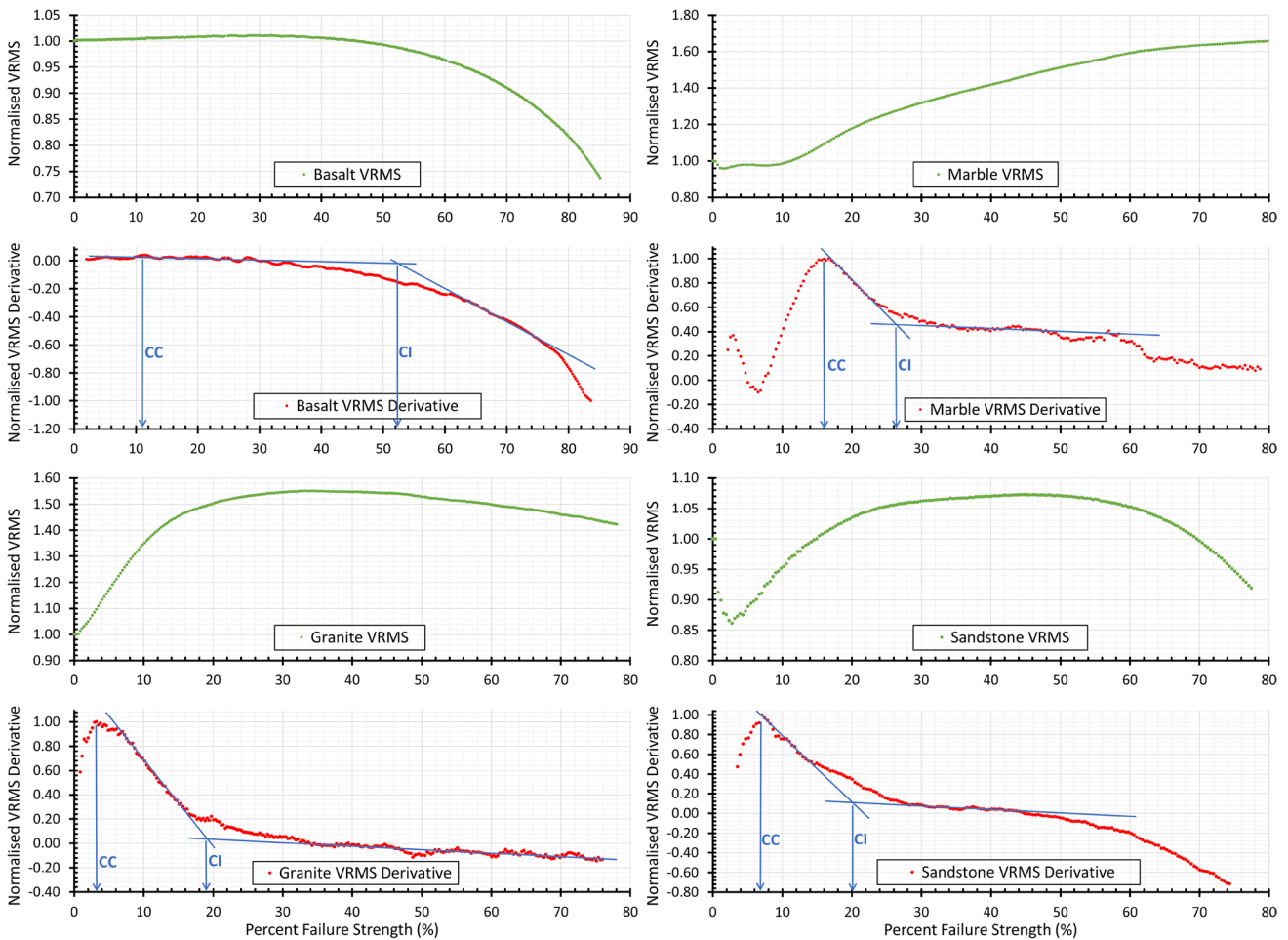

Fig. 8 Change in VRMS (green lines) and VRMS derivatives (red lines) during uniaxial loading for basalt (top left), marble (top right), granite (bottom left), and sandstone (bottom right) samples. The CC and CI stress thresholds are determined using blue reference lines on the derivative graphs
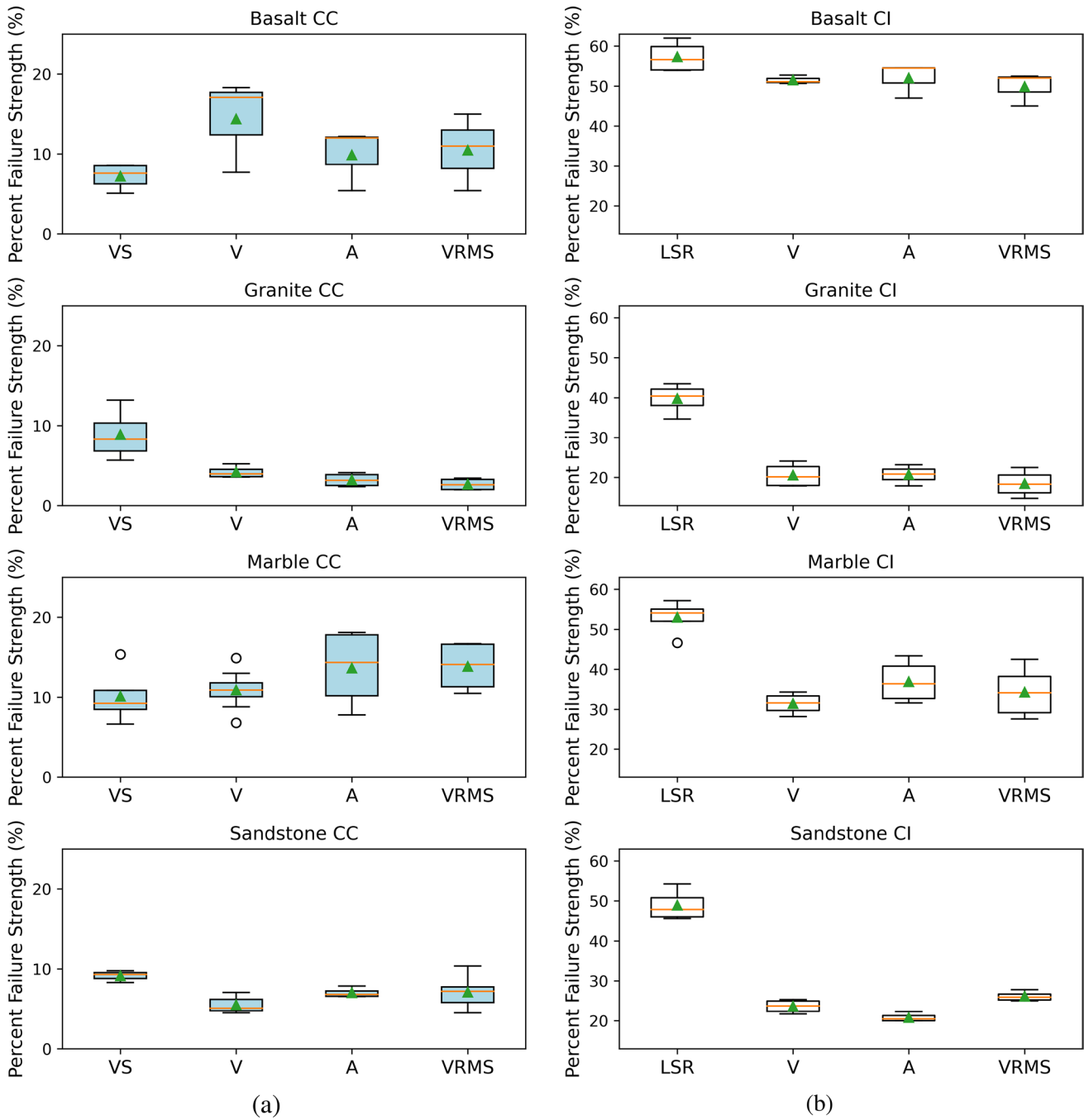
Fig. 9 Box plot comparison of the **a** CC stress threshold, and **b** CI stress threshold determined using Volumetric Strain (VS), Lateral Strain Response (LSR), ultrasonic velocity (V), ultrasonic amplitude (A), and ultrasonic VRMS analysis methods. Median and mean values are indicated by a horizontal orange line and a green triangle, respectively

methods and newly proposed ultrasonic methods. Since averaging the CC and CI values derived from all the six stress–strain methods might be misleading due to the different levels of subjectivity involved in each method, the VS and LSR results were preferred for comparison with ultrasonic results. The choice was made based on a higher

consistency and a smaller CoV among specimens using the VS and LSR results. According to Fig. 9:

(1)   There is a good agreement between CC and CI values estimated using the conventional stress–strain based methods and the three ultrasonic methods proposed in this study.

Table 5 Average and SD of the CC and CI stress thresholds determined using stress–strain methods and ultrasonic methods

Rock type	CC (% UCS)				CI (% UCS)			
	VS	V	A	VRMS	LSR	V	A	VRMS
Basalt	7.2 ± 1.4	14.4 ± 4.7	9.9 ± 3.2	10.5 ± 3.9	57.3 ± 3.4	51.5 ± 0.9	52.0 ± 3.5	49.8 ± 3.4
Granite	8.9 ± 2.8	4.2 ± 0.7	3.2 ± 0.8	2.6 ± 0.7	39.7 ± 3.3	20.6 ± 2.7	20.7 ± 2.0	18.5 ± 3.0
Marble	10.1 ± 3.2	10.9 ± 2.3	13.7 ± 4.4	13.9 ± 2.8	53.0 ± 3.9	31.4 ± 2.4	36.9 ± 4.5	34.2 ± 5.3
Sandstone	9.1 ± 0.6	5.5 ± 1.0	7.0 ± 0.5	7.1 ± 1.9	48.9 ± 3.5	23.6 ± 1.5	20.8 ± 0.9	26.1 ± 1.0

(2) All three ultrasonic proposed methods produce similar estimations of CC and CI.

(3) Compared to stress–strain-based methods, ultrasonic methods consistently yield lower estimates for CI in all rock types. This is attributed to the ultrasonics' ability to detect microcracks inside a loaded sample much earlier than strain gauges attached to the sample surface.

(4) When considering each ultrasonic methods individually, velocity analysis exhibits higher consistency across different specimens, characterised by a smaller inter quartile range and CoV. Amplitude analysis, on the other hand, shows more variation between specimens, reflected by a larger interquartile range, primarily due to its heightened sensitivity to microscopic changes, resulting in higher percentage changes during loading. The VRMS analysis, which incorporates changes in both amplitude and frequency, tends to provide a damage stress threshold within the range given by amplitude and frequency analysis, with a smaller variation. However, this method necessitates an understanding of both amplitude and frequency changes, and careful interpretation of the graph to account for local fluctuations, thereby introducing subjectivity and making replication more challenging.

(5) Additional statistical analysis using ANOVA was conducted in MATLAB to determine whether the damage stress thresholds determined using ultrasonic methods have a common mean. A higher P-value indicates less difference between the mean value of the two groups. If the P-value is smaller than a significance level (usually 0.05% or 5%), it can be concluded that the two group means are different (MathWorks 2022). Upon conducting ANOVA calculations (see Table 6, it can be checked that the majority of cases exhibit a P-value greater than the 0.05 threshold. This indicates that

there is no statistically significant difference between the means of ultrasonic groups.

(6) The above findings provide strong evidence supporting effectiveness of the proposed ultrasonic methods in detecting the evolution of damage in a loaded rock specimen, extending up to the point of failure.

4 Conclusions

This study aimed to assess the feasibility and accuracy of ultrasonic through-transmission methods in determining rock crack damage stress thresholds. Uniaxial compression tests were conducted on four different rock types, employing both strain measurement and active ultrasonic monitoring. Continuous recordings of three ultrasonic indicators—wave velocity, amplitude, and VRMS—were captured throughout the loading process using a pair of 2.25 MHz P-wave transducers. Results revealed distinct trends in the normalised percentage change of ultrasonic indicators for each rock type. However, a general trend can be observed when analysing the derivative (rate of change) of the ultrasonic indicators. The point of maximum derivative aligns closely with the crack closure (CC) stress threshold, while the intersection of two linear regions on the derivative graph can be used to characterise the crack initiation (CI) stress threshold. This derivative analysis method proved applicable to all three ultrasonic indicators across all tested rock types, underscoring the versatility and reliability of the proposed approach. In comparison to the crack damage stress thresholds determined using conventional stress–strain techniques, all three ultrasonic methods provide consistent estimations of the CC and CI stress thresholds with smaller variations between specimens. Importantly, ultrasonic methods also

Table 6 Statistical comparisons of the crack damage stress threshold determined using ultrasonic method

Item	Compared groups			P-value		Compared groups			P-value
Basalt CC	V	A	VRMS	0.509	Basalt CI	V	A	VRMS	0.742
Granite CC	V	A	VRMS	0.068	Granite CI	V	A	VRMS	0.514
Marble CC	V	A	VRMS	0.281	Marble CI	V	A	VRMS	0.262
Sandstone CC	V	A	VRMS	0.155	Sandstone CI	V	A	VRMS	0.001

provide earlier indications of the CI stress thresholds compared to the stress–strain methods. These results strongly indicate that the ultrasonic parameters introduced in this study can serve as a reliable alternative to relatively more time-consuming, subjective, and costly stress–strain methods for characterising crack damage stress thresholds, highlighting potential practical implications in the field of rock mechanics. Future research avenues may include monitoring crack damage (CD) stress thresholds, implementing an automated procedure for finding intersections to enhance robustness and objectivity, conducting transducer frequency sensitivity analyses, and exploring the effects of temperature, moisture, and different loading conditions. These enhancements aim to advance the applicability and reliability of the proposed ultrasonic methods, contributing to the broader application of ultrasonic testing methods for rock damage characterisation.

Declarations

Competing interests The authors declare that they have no conflict of interest.

References

Andersson JC, Martin CD, Stille H (2009) The Äspö pillar stability experiment: part ii-rock mass response to coupled excavation-induced and thermal-induced stresses. Int J Rock Mech Min Sci 46(5):879–895

Bieniawski Z (1967) Mechanism of brittle fracture of rock: part i-theory of the fracture process. Int J Rock Mech Min Sci 4(4):395–406

Bieniawski ZT, Bernede MJ (1979) Suggested methods for determining the uniaxial compressive strength and deformability of rock materials: Part 1. Suggested method for determining deformability of rock materials in uniaxial compression. Int J Rock Mech Min Sci Geomech Abstr 16(2):138–140

Brace WF, Paulding BW Jr, Scholz C (1966) Dilatancy in the fracture of crystalline rocks. J Geophys Res (1896-1977) 71(16):3939–3953

Cadoret T, Marion D, Zinszner B (1995) Influence of frequency and fluid distribution on elastic wave velocities in partially saturated limestones. J Geophys Res Solid Earth 100(B6):9789–9803

Cai M, Kaiser PK (2014) In-situ rock spalling strength near excavation boundaries. Rock Mech Rock Eng 47(2):659–675

Chang S-H, Lee C-I (2004) Estimation of cracking and damage mechanisms in rock under triaxial compression by moment tensor analysis of acoustic emission. Int J Rock Mech Min Sci 41(7):1069–1086

Chawre B (2018) Correlations between ultrasonic pulse wave velocities and rock properties of quartz-mica schist. J Rock Mech Geotech Eng 10(3):594–602

Dai J, Liu J, Zhou L, He X (2023) Real-time ultrasonic features and damage characterization of deep shale. Rock Mech Rock Eng 56(4):2535–2550

Diederichs MS (2007) The 2003 canadian geotechnical colloquium; mechanistic interpretation and practical application of damage and spalling prediction criteria for deep tunnelling. Can Geotech J 44(9):1082–1116

Eberhardt E, Stead D, Stimpson B, Read RS (1998) Identifying crack initiation and propagation thresholds in brittle rock. Can Geotech J 35(2):222–233

Entwisle DC, Hobbs PRN, Jones LD, Gunn D, Raines MG (2005) The relationships between effective porosity, uniaxial compressive strength and sonic velocity of intact borrowdale volcanic group core samples from sellafield. Geotech Geol Eng 23(6):793–809

Fairhurst C, Cook N (1966) The of maximum phenomenon of rock splitting parallel to the direction compression in the neighbourhood of a surface, ISRM

Felice MV, Fan Z (2018) Sizing of flaws using ultrasonic bulk wave testing: a review. Ultrasonics 88:26–42

Garg P, Shirole D, Hedayat A, Griffiths D (2019) Coupled ultrasonic and digital imaging of crack initiation and growth in prismatic Lyon sandstone rocks. In: ARMA US rock mechanics/geomechanics symposium (pp. ARMA-2019). ARMA

Ghazvinian E (2015) Fracture initiation and propagation in low porosity crystalline rocks: implications for excavation damage zone (edz) mechanics, Thesis, copyright - Database copyright ProQuest LLC; ProQuest does not claim copyright in the individual underlying works. Last updated 03-11-2022

Ji P-Q, Zhang X-P, Zhang Q (2018) A new method to model the nonlinear crack closure behavior of rocks under uniaxial compression. Int J Rock Mech Min Sci 112:171–183

Keneti A, Sainsbury BA (2018) Review of published rockburst events and their contributing factors. Eng Geol 246:361–373

Kim J-S, Lee K-S, Cho W-J, Choi H-J, Cho G-C (2015) A comparative evaluation of stress-strain and acoustic emission methods for quantitative damage assessments of brittle rock. Rock Mech Rock Eng 48(2):495–508

Koosmen K, Wang T, Asche H, Serati M (2023) Subjectivity in crack initiation measurements using conventional stress-strain based methods. In: 57th US Rock Mechanics/Geomechanics Symposium, Atlanta

Lajtai EZ (1974) Brittle fracture in compression. Int J Fract 10(4):525–536

Li BQ, Einstein HH (2017) Comparison of visual and acoustic emission observations in a four point bending experiment on barre granite. Rock Mech Rock Eng 50:2277–2296

Li BQ, Gonçalves da Silva B, Einstein H (2019) Laboratory hydraulic fracturing of granite: acoustic emission observations and interpretation. Eng Fract Mech 209:200–220

Martin C, Chandler N (1994) The progressive fracture of Lac du bonnet granite. Int J Rock Mech Min Sci 31(6):643–659

Martin C, Christiansson R (2009) Estimating the potential for spalling around a deep nuclear waste repository in crystalline rock. Int J Rock Mech Min Sci 46(2):219–228

Martin CD, Kaiser PK, McCreath DR (1999) Hoek-brown parameters for predicting the depth of brittle failure around tunnels. Can Geotech J 36(1):136–151

Masoumi H, Serati M, Williams D, Alehossein H (2017) Size dependency of intact rocks with high brittleness: a potential solution to eliminate secondary fractures in Brazilian test, 51st US Rock Mechanics/Geomechanics Symposium. California, San Francisco, p 0843

MathWorks (2022) Statistics and machine learning toolbox user's guide, Report, MathWorks

Modiriasari A, Bobet A, Pyrak-Nolte LJ (2017) Active seismic monitoring of crack initiation, propagation, and coalescence in rock. Rock Mech Rock Eng 50(9):2311–2325

Nicksiar M, Martin CD (2012) Evaluation of methods for determining crack initiation in compression tests on low-porosity rocks. Rock Mech Rock Eng 45(4):607–617

Nur A, Simmons G (1969) The effect of saturation on velocity in low porosity rocks. Earth Planet Sci Lett 7(2):183–193

Olympus (2019) Ultrasonic transducer catalog

Ortlepp W, Stacey T (1994) Rockburst mechanisms in tunnels and shafts. Tunn Undergr Space Technol 9(1):59–65

Pellet FL, Fabre G (2007) Damage evaluation with p-wave velocity measurements during uniaxial compression tests on argillaceous rocks. Int J Geomech 7(6):431–436

Pyrak-Nolte LJ, Myer LR, Cook NG (1990) Transmission of seismic waves across single natural fractures. J Geophys Res Solid Earth 95(B6):8617–8638

Ranjith PG, Zhao J, Ju M, De Silva RV, Rathnaweera TD, Bandara AK (2017) Opportunities and challenges in deep mining: a brief review. Engineering 3(4):546–551

Saltas V, Fitilis I, Vallianatos F (2014) A combined complex electrical impedance and acoustic emission study in limestone samples under uniaxial loading. Tectonophysics 637:198–206

Serati M, Alehossein H, Williams D (2012) Elastic stress analysis of partially loaded hollow discs. Int J Eng Sci 53:19–37

Serati M, Alehossein H, Williams D (2014) 3D elastic solutions for laterally loaded discs: generalised Brazilian and point load tests. Rock Mech Rock Eng 47:1087–1101

Serati M, Alehossein H, Williams DJ (2015) Estimating the tensile strength of super hard brittle materials using truncated spheroidal specimens. J Mech Phys Solids 78:123–140

Serati M, Jakson N, Asche H, Basireddy S, Malgotra G (2022) Sustainable shotcrete production with waste glass aggregates. SN Appl Sci. https://doi.org/10.1007/s42452-022-04967-4

Serati M, Wang T, Koosmen K (2022a) Crack initiation and damage evolution in high porosity sandstone under cyclic compression. In: 10th international symposium on rockbursts and seismicity in mines, Tucson

Shirole D, Hedayat A, Ghazanfari E, Walton G (2020) Evaluation of an ultrasonic method for damage characterization of brittle rocks. Rock Mech Rock Eng 53(5):2077–2094

Shirole D, Hedayat A, Walton G (2020) Illumination of damage in intact rocks by ultrasonic transmission-reflection and digital image correlation. J Geophys Res Solid Earth 125(7):e2020JB019e2020JB019526

Shuai W, Ying X, Yanbo Z, Xulong Y, Peng L, Xiangxin L (1997) Effects of sandstone mineral composition heterogeneity on crack initiation and propagation through a microscopic analysis technique. Int J Rock Mech Min Sci (Oxf Engl) 162(2023):105307

Stacey T (1981) A simple extension strain criterion for fracture of brittle rock. Int J Rock Mech Min Sci 18(6):469–474

Stanchits S, Vinciguerra S, Dresen G (2006) Ultrasonic velocities, acoustic emission characteristics and crack damage of basalt and granite. Pure Appl Geophys 163(5):975–994

Wu R, Selvadurai PA, Chen C, Moradian O (2021) Revisiting piezoelectric sensor calibration methods using elastodynamic body waves. J Nondestr Eval 40(3):68

Wu R, Selvadurai PA, Li Y, Sun Y, Leith K, Loew S (2023) Laboratory acousto-mechanical study into moisture-induced changes of elastic properties in intact granite. Int J Rock Mech Min Sci 170:105511

Wulff A-M, Hashida T, Watanabe K, Takahashi H (1999) Attenuation behaviour of tuffaceous sandstone and granite during microfracturing. Geophys J Int 139(2):395–409

Yang S, Nong Z, Feng X, Kan J, Pan D, Qian D (2018) Experimental investigation of sandstone under cyclic loading: damage assessment using ultrasonic wave velocities and changes in elastic modulus. Shock Vib 2018:1–13

Yin D, Xu Q (1997) Investigating the damage evolution of sandstone using electrical impedance spectroscopy,. Int J Rock Mech Min Sci (Oxf Engl) 144(2021):104817

Yin D, Xu Q (2020) Comparison of sandstone damage measurements based on non-destructive testing. Materials 13(22):5154

Zhang X-P, Lv G-G, Liu Q-S, Wu S-C, Zhang Q, Ji P-Q, Tang X-H (2021) Identifying accurate crack initiation and propagation thresholds in siliceous siltstone and limestone. Rock Mech Rock Eng 54(2):973–980

Zhao XG, Cai M, Wang J, Ma LK (2013) Damage stress and acoustic emission characteristics of the Beishan granite. Int J Rock Mech Min Sci 64:258–269

Zhao XG, Cai M, Wang J, Li PF, Ma LK (2015) Objective determination of crack initiation stress of brittle rocks under compression using AE measurement. Rock Mech Rock Eng 48(6):2473–2484